TISSUE ENGINEERING: Part A
Volume 21, Numbers 1 and 2, 2015

DOI: 10.1089/ten.tea.2013.0775

Experimental and Computational Investigation of the Effect of Hydrophobicity on Aggregation and Osteoinductive Potential of BMP-2-Derived Peptide in a Hydrogel Matrix

Seyedsina Moeinzadeh, BS, Danial Barati, MS, Samaneh K. Sarvestani, MS, Tahereh Karimi, PhD, and Esmaiel Jabbari, PhD

An attractive approach to reduce the undesired side effects of bone morphogenetic proteins (BMPs) in regenerative medicine is to use osteoinductive peptide sequences derived from BMPs. Although the structure and function of BMPs have been studied extensively, there is limited data on structure and activity of BMP-derived peptides immobilized in hydrogels. The objective of this work was to investigate the effect of concentration and hydrophobicity of the BMP-2 peptide, corresponding to residues 73–92 of the knuckle epitope of BMP-2 protein, on peptide aggregation and osteogenic differentiation of human mesenchymal stem cells encapsulated in a polyethylene glycol (PEG) hydrogel. The peptide hydrophobicity was varied by capping PEG chain ends with short lactide segments. The BMP-2 peptide with a positive index of hydrophobicity had a critical micelle concentration (CMC) and formed aggregates in aqueous solution. Based on simulation results, there was a slight increase in the concentration of free peptide in solution with 1000-fold increase in peptide concentration. The dose-osteogenic response curve of the BMP-2 peptide was in the 0.0005–0.005 mM range, and osteoinductive potential of the BMP-2 peptide was significantly less than that of BMP-2 protein even at 1000-fold higher concentrations, which was attributed to peptide aggregation. Further, the peptide or PEG-peptide aggregates had significantly higher interaction energy with the cell membrane compared with the free peptide, which led to a higher nonspecific interaction with the cell membrane and loss of osteoinductive potential. Conjugation of the BMP-2 peptide to PEG increased CMC and osteoinductive potential of the peptide whereas conjugation to lactide-capped PEG reduced CMC and osteoinductive potential of the peptide. Experimental and simulation results revealed that osteoinductive potential of the BMP-2 peptide is correlated with its CMC and the free peptide concentration in aqueous medium and not the total concentration.

Introduction

A feasible approach to the restoration of injured bone tissue is the use of tissue engineering strategies to transplant undifferentiated human mesenchymal stem cells (hMSCs) in a supportive carrier loaded with bone morphogenetic proteins (BMPs). In particular, human recombinant BMP-2 is used extensively in certain clinical applications, such as spine fusion, sinus augmentation, and alveolar ridge augmentation, to accelerate bone regeneration and healing.[1] Due to its short half-life and diffusion of the protein away from the site of regeneration, doses much higher than the endogenous amount are loaded in the implant to induce bone formation.[1,2] High doses of BMP-2 protein *in vivo* cause undesired side effects, such as bone overgrowth, immune response, and tumorigenesis.[3] For example, the probability of an adverse side effect with the use of BMP-2 in spine fusion may be as high as 40%.[3] Encapsulation or grafting of nano- and microspheres is used to localize the protein to the site of regeneration and reduce diffusion[4–6]; however, tumor formation and inflammatory response persist in some patients.[7]

The side effects of BMP-2 protein stem from its ability to promote cell migration and vascularization and its involvement in tumor angiogenesis.[8] Therefore, an attractive approach to reduce the side effects of protein in bone tissue engineering is to use peptides derived from the bioactive domains of BMP-2 and other morphogenetic proteins.[9] BMP-2 protein is a homodimer of two 114-amino-acid residues with two distinct epitopes. The wrist epitope is assembled around the central α-helix while the knuckle epitope is located on the two aligned double-stranded β-sheets.[10,11] It has been shown that the activity of BMP-2 protein is mainly due to the interaction of the knuckle epitope with type II BMP

Biomimetic Materials and Tissue Engineering Laboratory, Department of Chemical Engineering, University of South Carolina, Columbia, South Carolina.

receptor (BMP-II).[10] Multiple peptides derived from the knuckle epitope of BMP-2 protein have been shown to have osteoinductive potential.[12,13] Among those, a peptide corresponding to residues 73–92 (hereinafter referred to as BMP-2 peptide) showed highest alkaline phosphatase (ALP) and osteogenic differentiation of MSCs, but the peptide activity was significantly lower than BMP-2 protein.[9] The higher activity of the protein compared with the BMP-2 peptide may be due to conformational differences between the native and free states of the peptide in aqueous medium. Peptides have recently been used to generate tubular, fibrillar, micellar, or vesicular nanostructures due their amphiphilic nature.[14–17] For example, peptides with a hydrophilic head and a hydrophobic tail spontaneously self-assemble to form vesicular structures in aqueous solution.[18] Peptide aggregation may alter the overall conformation and presentation of the amino acid sequence that interacts with cell surface receptors, which adversely affects the osteoinductive potential of the peptide. Although the structure and activity of BMP-2 protein has been extensively investigated *in vitro* and *in vivo*, there is limited data on aggregation and nanostructure formation by osteogenic peptides in aqueous solution and its effect on osteogenesis.

The objective of this work was to investigate the effect of concentration and hydrophobicity of the BMP-2 peptide on peptide aggregation and differentiation of hMSCs encapsulated in an inert polyethylene glycol (PEG) hydrogel. To test the effect of BMP-2 peptide on differentiation, the encapsulated hMSCs were cultured in osteogenic medium (OM) without dexamethasone (DEX). Molecular dynamic simulation was used to predict the effect of concentration and hydrophobicity on peptide aggregation and critical micelle concentration (CMC) using a MARTINI coarse-grained force field.[19–21] The peptide concentration was varied by 20,000-fold from 0.00025 to 5 mM with BMP-2 protein as the positive control. Hydrophobicity of the peptide was varied by capping PEG chain ends with 0–6 lactide monomers. PEG as an inert matrix with tunable properties[22–24] was used for encapsulation of hMSCs to isolate and investigate the effect of BMP-2 peptide hydrophobicity on its osteoinductive potential. Experimental and simulation results revealed that osteoinductive potential of the BMP-2 peptide is correlated with its CMC and the concentration of free peptide in aqueous medium and not the total peptide concentration.

Materials and Methods

Reagents

Linear PEG with nominal molecular weight of 3.4 kDa was purchased from Acros (Pittsburg, PA). Lactide (L) monomer with >99.5% purity was purchased from Ortec (Easley, SC) and it was dried under vacuum at 40°C for at least 12 h prior to use. 4-(2-Hydroxyethoxy)phenyl-(2-hydroxy-2-propyl) ketone (Irgacure-2959) photoinitiator was obtained from CIBA (Tarrytown, NY). The protected amino acids and Rink Amide NovaGel™ resin were purchased from EMD Biosciences (San Diego, CA). Piperidine, calcium hydride, tetrahydrofuran (THF), trimethylsilane (TMS), triethylamine (TEA), tin (II) 2-ethylhexanoate (TOC), acryloyl chloride (AC), acrylic acid, dimethylsulfoxide (DMSO), and ethylenediaminetetraacetic acid (EDTA) disodium salt were purchased from Sigma-Aldrich (St. Louis, MO). Dichloromethane (DCM; Acros) was dried by distillation over calcium hydride. Other solvents were obtained from VWR (Bristol, CT) and used as received. The protected amino acids and Rink Amide NovaGel resin for peptide synthesis were purchased from EMD Biosciences. N,N-dimethylformamide (DMF), acetonitrile (MeCN), N,N-diisopropylethylamine (DIEA), N,N′-diisopropylcarbodiimide (DIC), triisopropylsilane (TIPS), N,N-dimethylaminopyridine (DMAP), hydroxybenzotriazole (HOBt), and trifluoroacetic acid (TFA) were received from Acros. Dulbecco's phosphate-buffer saline (PBS) and Dulbecco's modified Eagle's medium (DMEM; 4.5 g/L glucose with L-glutamine and without sodium pyruvate) were received from GIBCO BRL (Grand Island, NY). Fetal bovine serum (FBS) was purchased from Atlas Biologicals (Fort Collins, CO). TRIzol for isolation of cellular RNA and trypsin were purchased from Invitrogen (Carlsbad, CA). Penicillin (PN), streptomycin (SP), fungizone (FG), gentamicin sulfate (GS), DEX, ascorbic acid (AA), and β-sodium glycerophosphate (βGP) were purchased from Sigma-Aldrich. Quant-it PicoGreen dsDNA reagent kit was obtained from Invitrogen. QuantiChrom calcium and ALP assay kits were purchased from Bioassay Systems (Hayward, CA). hMSCs, harvested and cultured from normal human bone marrow, were purchased from Lonza (Allendale, NJ). The cells were tested for purity by high expression of CD105, CD166, CD29, and CD44 and low expression of CD14, CD34, and CD45 markers as described by the supplier (Lonza).

Synthesis of lactide-capped PEG macromer

The PEG macromer was capped with short lactide segments (<6 monomers) by condensation polymerization as we previously described.[23,25] Briefly, the residual moisture was removed from the PEG macromer by azeotropic distillation from toluene. The PEG macromer and lactide monomers were heated to 120°C under dry nitrogen atmosphere in a reaction flask equipped with an overhead stirrer. After melting, 1 mL of TOC catalyst was added and the reaction was allowed to proceed for 8 h at 135°C. After the reaction, the product was dissolved in DCM and precipitated in ice-cold methanol, followed by precipitation in ether and hexane to remove the unreacted monomer and PEG. Then, the product was dried in vacuum and stored at −20°C. In the next step, the lactide-capped PEG was functionalized by reaction with AC using the following procedure. Equimolar amounts of AC and TEA were added dropwise to a cooled solution of the capped macromer in DCM and the reaction was allowed to continue for 12 h. After the reaction, solvent was removed by rotary evaporation and the residue was redissolved in ethyl acetate to precipitate the byproduct triethylamine hydrochloride salt. Next, ethyl acetate was removed by vacuum distillation and the functionalized macromer was dissolved in DCM and precipitated twice in ice-cold ethyl ether. The product was dissolved in DMSO, purified by dialysis, freeze dried, and stored at −20°C. A similar procedure was used for functionalization of PEG to produce PEG diacrylate (PEG-DA) macromer. The synthesized macromers were characterized by hydrogen nuclear magnetic resonance (^{1}H-NMR) (Varian, Palo Alto, CA) as we previously described.[25] The synthesized macromer is hereinafter referred to as L*n* where ''L'' stands for lactide-capped PEG macromer and ''*n*'' is the number of lactide monomers per chain end.

BMP-2 peptide synthesis and conjugation to the macromer

The amino acid sequence KIPKA SSVPT ELSAI STLYL (BMP-2 peptide, Fig. 1a) was synthesized manually on Rink Amide NovaGel resin in the solid phase as we previously described.[24] The pseudoproline dipeptides (oxazolidine) Fmoc-Ser(tBu)-Thr($\Psi^{Me,Me}$pro)-OH, Fmoc-Leu-Ser($\Psi^{Me,Me}$pro)-OH, and Fmoc-Ala-Ser($\Psi^{Me,Me}$pro)-OH were used in the peptide synthesis to improve the coupling efficiency and product yield.[26] Briefly, the Fmoc-protected amino acid (1 equiv), HOBt (2 equiv), and DIC (1.1 equiv) were added to 100 mg resin swelled in DMF. Next, 0.2 mL of 0.05 M DMAP was added to the mixture and the coupling reaction was allowed to proceed for 4–6 h at 30°C with orbital shaking. After each coupling reaction, the resin was tested for the presence of unreacted amines using the Kaiser reagent.[27] The coupling reaction was repeated if the test result was positive. Otherwise, the resin was treated with 20% piperidine in DMF and the next Fmoc-protected amino acid was coupled. For direct conjugation of BMP-2 peptide to the hydrogel matrix, acrylamide-terminated BMP-2 peptide was synthesized by the reaction between N-terminal amine of the peptide with acrylic acid directly on the resin under reaction conditions used for amino acid coupling. Acrylamide-terminated cell-adhesive GRGD peptide (Ac-GRGD) was synthesized using a similar procedure. For conjugation of the peptide to lactide-capped PEG macromer, the amino acid sequence cysteine-glycine-glycine was coupled to the lysine end of the BMP-2 peptide directly on the resin. After coupling the last amino acid, the peptide was cleaved from the resin by treating with 95% TFA/2.5% TIPS/2.5% water for 2 h and precipitated in cold ether. The peptide was further purified by preparative HPLC and characterized by electrospray ionization mass spectrometry as we previously described.[24]

The Michael addition reaction between the cysteine's sulfhydryl group on the peptide and the acrylate on the macromer was used for conjugation, similar to a procedure we previously described.[28] Figure 1a and b shows the bead structure of the BMP-2 peptide and peptide-macromer conjugate, respectively. Blue, brown, and green beads in Figure 1b represent acrylate, lactide, and ethylene oxide (EO) units of the macromer, respectively. Briefly, a solution of the peptide in sodium borate buffer was added to the solution of macromer in DMF in a 1:1 molar ratio to terminate on average one end of the macromer with peptide and leaving the unreacted acrylate-terminated end for attachment to the hydrogel matrix. The conjugation reaction was allowed to proceed for 24 h at 30°C. After the reaction, the solution was dialyzed against distilled deionized water to remove the unreacted monomer and peptide, and freeze dried to obtain the dry peptide-macromer conjugate. The number of peptides per lactide-capped PEG chain was determined by ^{1}H-NMR as we described previously.[28] The conjugate is hereinafter referred to as PL*n* where "P," "L," and "*n*" stand for BMP-2 peptide, lactide-capped PEG macromer, and number of lactide monomers per chain end, respectively.

Dynamic light scattering

Dynamic light scattering (DLS) was used to determine CMC of the peptide as described.[29] Solutions with different concentrations of the peptide in PBS were prepared by sonication for 10 min. A 20 µL aliquot of the peptide solution was used for DLS measurements on a DynaPro MSX DLS instrument (Wyatt Technology, Santa Barbara, CA). The intensity of scattered light at 90° angle was collected and averaged over 50 data points using the DynaPro software (Wyatt Technology). Intersection of the two linear lines fitted to the data for scattered light intensity at low and high concentrations was used to define CMC for the peptide as previously described.[30]

Cell encapsulation and culture

Prior to cell encapsulation, hMSCs were cultivated at 5000 cells/cm^2 in a high-glucose DMEM supplemented with 10% FBS, 100 units/mL PN, and 100 µg/mL SP. The medium was

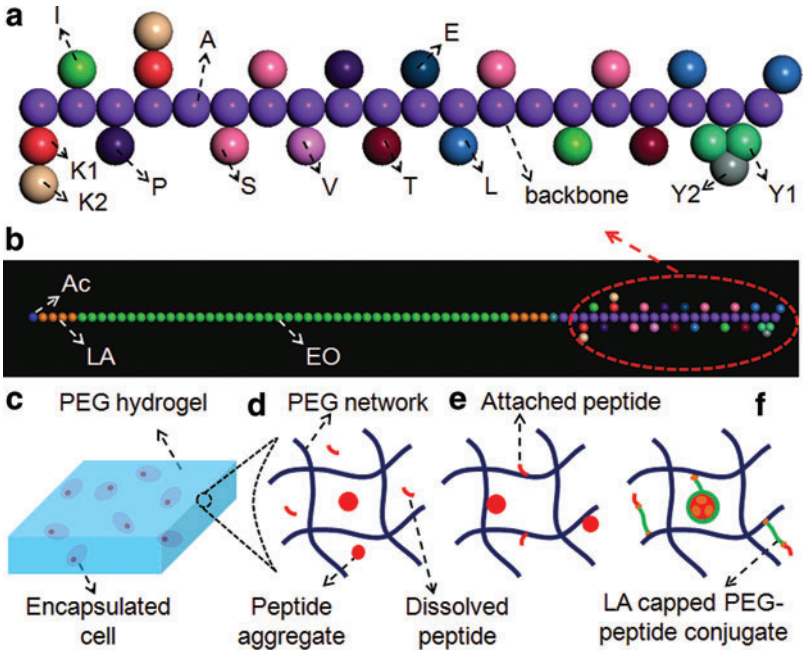

FIG. 1. Bead representation of the bone morphogenetic protein (BMP)-2 peptide **(a)** and the peptide/lactide-capped polyethylene glycol (PEG) conjugate **(b)**. Lactide, ethylene oxide, and acrylate units in **(b)** are shown in *brown*, *green*, and *blue beads*, respectively. **(c)** Schematic representation of human mesenchymal stem cells (hMSCs) encapsulated in the PEG diacrylate (PEGDA) (*blue network*) hydrogel matrix for all groups. Experimental groups included the peptide (shown in *red*) dissolved in the hydrogel network **(d)**, peptide covalently attached to the hydrogel network **(e)**, and peptide/lactide-capped PEG conjugate attached to the hydrogel network **(f)**. The *red lines* and *circles* in **(d–f)** represent the peptide chain and peptide aggregate, respectively. The lactide-capped PEG macromer in **(f)** is shown by *brown-green* colors. Color images available online at www.liebertpub.com/tea

refreshed every 3 days. When the cultivated hMSC colonies reached ~70% confluency, the cells were detached with 0.1% trypsin-0.03% EDTA and subcultivated at 1:3 ratio. According to supplier's instructions (Lonza), all hMSCs used in cell culture experiments were passaged <5 times. The following procedure was used for encapsulation of hMSCs in BMP-2-peptide-incorporated PEGDA hydrogels by UV polymerization, as shown in Figure 1c.[22,25] First, BMP-2 peptide, with or without conjugation to the lactide-capped macromer, was dissolved in a solution of Irgacure-2959 photoinitiator (1 wt% of PEGDA) in PBS. Next, 1 wt% Ac-GRGD adhesive peptide was dissolved in a solution of PEGDA macromer (15 wt%) in PBS to improve cell viability and cell–matrix interaction after encapsulation. After sterilization by filtration, the initiator and macromer solutions were mixed by vortexing for 5 min to generate the hydrogel precursor solution. Then, 1×10^6 hMSCs, suspended in 100 μL PBS, were added to the precursor solution and mixed gently with a presterilized glass rod. The suspension of cells in the precursor solution was injected between two sterile microscope glass slides and crosslinked by UV irradiation with a BLAK-RAY 100-W mercury, long-wavelength (365 nm) UV lamp (Model B100-AP; UVP, Upland, CA) as we described previously.[31] The final density of hMSCs in the PEGDA gel was 2×10^6 cells/mL. Experimental groups included peptide dissolved in PEGDA gel (Fig. 1d, peptide in red), peptide covalently attached to PEGDA gel (Fig. 1e), and peptide/lactide-capped PEG conjugate attached to PEGDA gel (Fig. 1f). Abbreviations ''P'' and ''cP'' denote BMP-2 peptide dissolved in and conjugated to PEGDA hydrogel, respectively; ''PL*n*'' denotes BMP-2 attached to lactide-capped macromer and dissolved in PEGDA gel; and ''cPL*n*'' denotes BMP-2 peptide attached to lactide-capped macromer and conjugated to PEGDA gel. After removing from the glass slide and cutting the gel with a cork borer, the disk-shaped samples were incubated in basal medium (BM) for 24 h with two medium changes. The medium was then replaced with OM without DEX (50 μg/mL AA and 10 mM βGP) and incubated for 28 days. The cell-encapsulated gels (without BMP-2 peptide) incubated in BM and OM without DEX were used as negative controls while those with 0.0004 mM BMP-2 protein dissolved in the gel (and medium) was used as the positive control.[32,33] For the groups with peptide dissolved in the gel, the peptide was also added to the culture medium for concentration uniformity.

Biochemical and mRNA analysis

At each time point, the samples were divided in two groups. One group was homogenized and sonicated to rupture the membrane of the encapsulated cells and expose the DNA. Double-stranded DNA (dsDNA) content of the homogenized samples was analyzed using the PicoGreen assay as described.[25] Analysis of dsDNA was performed using a Synergy HT plate reader (Bio-Tek, Winooski, VT) with emission and excitation wavelengths of 485 and 528 nm, respectively. ALP activity of the samples was measured using the QuantiChrom ALP assay kit on a Synergy HT plate reader at the wavelength 405 nm as described.[25] The measured intensity was correlated to ALP activity in IU/L and normalized to cell numbers. Calcium content of the samples, as a measure of the total mineralized deposit, was measured using the QuantiChrom calcium assay kit as described.[25] The absorbance was measured on a Synergy HT plate reader at the wavelength of 575 nm. Measured intensities were correlated to the amount of equivalent Ca^{2+} using a calibration curve made with calcium chloride solutions of known concentrations. For mRNA analysis, total cellular RNA was isolated using TRIzol as described.[24] Two hundred fifty nanograms of the extracted total RNA was subjected to cDNA conversion using Promega reverse transcription system (Madison, WI). The obtained cDNA was subjected to real-time quantitative polymerase chain reaction (rt-qPCR) amplification with SYBR green RealMasterMix (Eppendorf, Hamburg, Germany) using Bio-Rad CXF96 PCR system (Bio-Rad, Hercules, CA) and the appropriate gene-specific primers. PCR experiments were performed to analyze the differential expression of osteogenic markers ALP and RunX-2 with time for hMSCs encapsulated in the gels. Primers for rt-qPCR were designed and selected using the Primer3 web-based software as described.[34] The following forward and reverse primers were synthesized by Integrated DNA Technologies (Coralville, IA): *ALP*: forward 5′-ATG GGA TGG GTG TCT CCA CA-3′ and reverse 5′-CCA CGA AGG GGA ACT TGT C-3′; *RunX-2*: forward 5′-ATG ACA CTG CCA CCT CTG A-3′ and reverse 5′-ATG AAA TGC TTG GGA ACT GC-3′; *GAPDH*: forward 5′-CAT GAC AAC TTT GGT ATC GTG G-3′ and reverse 5′-CCT GCT TCA CCA CCT TCT TG-3′.[35] The model of Pfaffl was used to determine the expression ratio of the gene.[36] The expression of *GAPDH* housekeeping gene was used as the reference, and the fold difference in gene expression was normalized to the first time point.

Statistical analysis

Data are expressed as means ± standard deviation. All experiments were done in triplicate. Significant differences between groups were evaluated using a two-way ANOVA with replication test, followed by a two-tailed Student's *t*-test. A value of $p < 0.05$ was considered statistically significant.

Simulation method

The atomistic structure of the BMP-2 peptide and lactide-capped PEG macromer was coarse-grained into different beads (set of atoms) using the MARTINI coarse graining model.[20,21] The MARTINI force field has been parameterized and applied previously to the simulation of proteins, peptides, polymers, and polymer-peptide conjugates.[37–42] This model is based on the four-to-one mapping with each bead in the coarse-grained model representing four heavy atoms in the atomistic model. The coarse graining of the peptide and macromer is schematically illustrated in Figure 1a. There were a total of 16 bead types for the peptide backbone, amino acid side chains, EO repeat unit, acrylate group (Ac), and lactide repeat unit (L). Each amino acid was coarse grained into a backbone bead and between zero to three side chain beads, based on the original MARTINI model developed for simulation of proteins.[20,21] After coarse graining, the beads were assigned pairwise interactions that included polar (PO), nonpolar (N), apolar (C), and charge (Q) interactions. To accurately represent its real nature, the interactions were grouped into subtypes based on the extent of hydrogen bonding or the degree of polarity of the beads. The polar beads were divided into five subtypes

based on the degree of polarity from low (PO1) to high (PO5). Apolar beads were divided into five subtypes from high (C1) to low apolar (C5). The nonpolar as well as charged beads were divided into four subtypes, namely, hydrogen donor, hydrogen acceptor, hydrogen donor and acceptor, and incapable of hydrogen bonding. For example, four water molecules were represented by a polar bead with degree of polarity of 4 or PO4. For nonbonded interactions, the following Lennard-Jones potential function V_{LJ} (r) was used.[21]

$$V_{LJ}(r) = 4\varepsilon_{ij}\left[\left(\frac{\sigma_{ij}}{r}\right)^{12} - \left(\frac{\sigma_{ij}}{r}\right)^{6}\right] \quad (1)$$

Where ε_{ij} is the depth of the potential well that is related to the strength of interaction between beads i and j, and σ_{ij} is the minimum distance of approach between beads i and j. To account for electrostatic interaction between charged beads, the following columbic function was used.[21]

$$V_{EL} = \frac{q_i q_j}{4\pi\varepsilon_0\varepsilon_{rel} r_{ij}} \quad (2)$$

Where q_i and q_j are values of the point charges on beads i and j, ε_0 is the dielectric constant of free space, and ε_{rel} is the relative dielectric constant of the medium. To account for interaction between bonded beads, the following potential functions were used: harmonic function (V_b) for bond length, cosine harmonic function (V_a) for bond angle, and dihedral function (V_d) for bond torsion.[21]

$$V_b = \frac{1}{2}K_b(r_{ij} - d_b)^2 \quad (3)$$

$$V_a = \frac{1}{2}K_a[(\cos(\theta_{ijk}) - \cos(\theta_a)]^2 \quad (4)$$

$$V_d = K_d[1 + \cos(n\psi_{ijkl} - \psi_d)] \quad (5)$$

Where K_b, K_a, and K_d are force constants for bond stretching, bond angle bending, and bond torsional rotation, respectively. r_{ij}, θ_{ijk}, and ψ_{ijkl} represent the distance between bonded beads i and j, the angle between bonded beads i, j, and k, and the dihedral angle between beads i, j, k, and l, respectively. d_b, θ_a, ψ_d, and n are the equilibrium bond length, bond angle, phase angle, and periodicity, respectively. Simulations were performed under canonical ensemble with conserved moles, volume, and temperature (NVT) ensemble dynamics. A time step of 10 fs was employed and the total simulation time was 5 μs. The temperature was held at 37°C using the Nose thermostat.[43] The simulations were performed in a $200\times200\times200$ Å box with 3D periodic boundary conditions. To cover a broader range of concentrations, a bigger $400\times400\times400$ Å box was used to simulate the effect of peptide concentration. The Mesocite module of Materials Studio (v5.5, Accelrys) was used for the mesoscale simulations.[44]

For simulations to investigate the interaction of BMP-2 peptide with the cell membrane, a template membrane with a width of 40 Å was generated using dipalmitoylphosphatidylcholine (DPPC) lipid as one face of the simulation box with the box filled with water. The coarse graining of DPPC has been described elsewhere.[45] The cell membrane was simulated under NVT ensemble for 100 ns to form the bilayer structure. After forming the lipid bilayer, the other components of system (peptide or peptide-macromer conjugate) were added to the simulation box. Next, the interaction type of all lipid bilayer beads was constrained to PO4 type in order to account for the interaction with water beads. Then, dynamic simulations were run for 5 μs to allow the formation of peptide or peptide-macromer aggregates in aqueous solution similar to the simulations without the lipid bilayer membrane. Next, the constraint was removed from the membrane beads and the pairwise bead interaction potential was changed accordingly. Finally, the system was simulated for 5 μs similar to that without the lipid bilayer membrane.

Results

The average number of lactides per chain end of lactide-capped PEG, average number of acrylates per chain end, and average number of BMP-2 peptides per conjugate was determined from the NMR spectra of macromers as we previously described.[25,28] The number of lactide repeat units per chain end of the lactide-capped PEG macromer was determined from the ratio of the peaks at 1.6 and 5.2 ppm (lactide hydrogens) to those at 3.6 and 4.3 ppm (PEG hydrogens).[25] The average number of lactide repeat units per chain end for L2, L4, and L6 macromers was 1.9, 3.6, and 5.6, respectively. The number of reactive acrylate groups per chain end was determined from the ratio of the peaks between 5.85 and 6.55 ppm (acrylate hydrogens) to those at 3.6 and 4.2 ppm (PEG hydrogens).[25] The average number of acrylates per chain end before peptide conjugation for L0, L2, L4, and L6 macromers was 0.85, 0.85, 0.83, and 0.82, respectively. The number of peptides in a peptide/lactide-capped PEG conjugate was determined using the acrylate/PEG molar ratios before and after conjugation as previously described.[28] The average number of peptides per conjugate for L0, L2, L4, and L6 macromers was 0.57, 0.49, 0.52, and 0.45, respectively. Several studies have demonstrated that >95% of acrylated PEG/peptide conjugates are integrated in PEGDA hydrogel network during photocrosslinking.[24,46,47]

Figure 2(a–e) shows the effect of dissolved (not attached to the gel network) BMP-2 peptide concentration on osteogenic differentiation of hMSCs encapsulated in the PEGDA hydrogel incubated in OM without DEX. Peptide concentration ranged from 0.00025 to 5 mM. Negative and positive control groups were gels without peptide and with 0.0004 mM BMP-2 protein, respectively. The clinically used concentration of BMP-2 protein is 1 mg/mL ($\sim$0.04 mM)[48] but the typical concentration used for *in vitro* 3D experiments is in the 1–10 μg/mL ($\sim$0.00004–0.0004 mM) range.[32,33] In this work, the upper concentration of 0.0004 mM was used to elucidate the effect of peptide on differentiation of hMSCs. DNA content, ALP activity, and calcium content of the groups are shown at a single time point (7, 14, and 21 days, respectively) in Figure 2a–c. DNA content of the groups at day 7 did not change appreciably with peptide concentration (Fig. 2a). ALP activity of hMSCs in the gel for all peptide concentrations reached a maximum on day 14 consistent with the biphasic activity of ALP in osteogenic differentiation of MSCs.[49] ALP activity of the encapsulated hMSCs at day 14 did not change significantly as the peptide concentration in the gel was increased from 0 to 0.00025 and

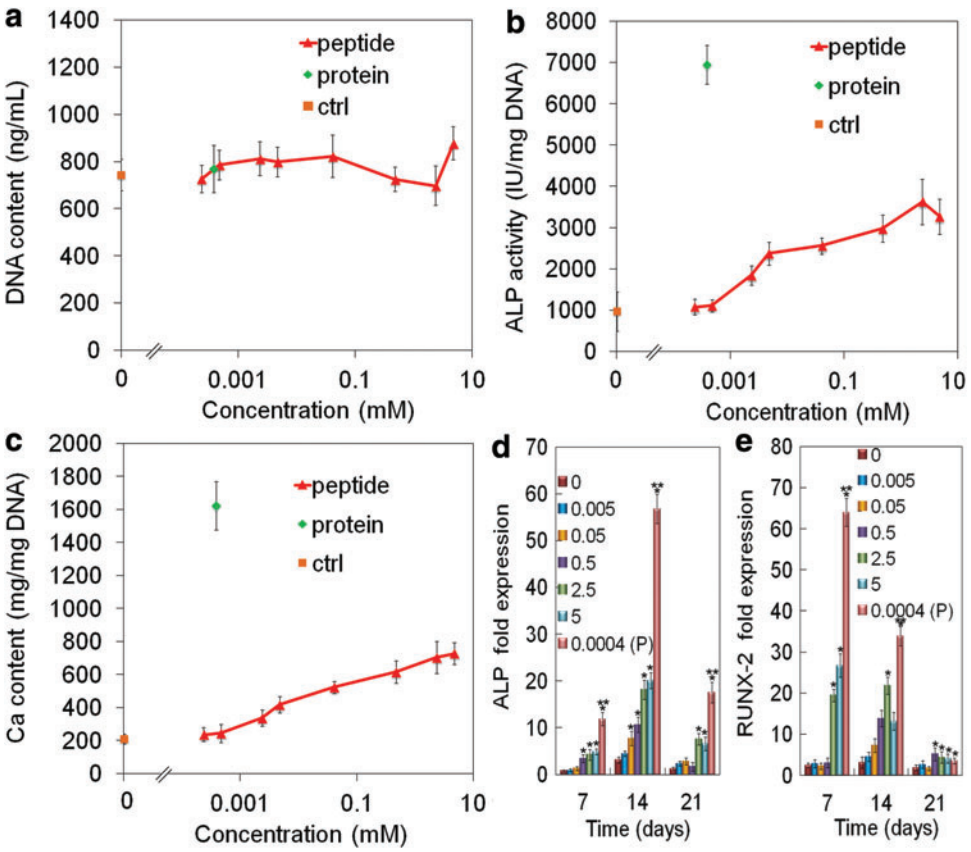

FIG. 2. DNA content **(a,** day 7), alkaline phosphatase (ALP) activity **(b,** day 14), and calcium content **(c,** day 21) of hMSCs encapsulated in PEGDA hydrogel (15 wt%) and incubated in osteogenic medium (OM) without dexamethasone (DEX) as a function of dissolved BMP-2 peptide concentration in the hydrogel matrix. Control groups included hMSCs encapsulated in PEGDA hydrogel (15 wt%) and cultured in OM without DEX and without the BMP-2 peptide (0 mM, negative control) and those cultured in OM with 0.0004 mM BMP-2 protein (0.01 Pr, positive control). Effect of the BMP-2 peptide concentration on ALP **(d)** and RunX-2 **(e)** mRNA marker expression of hMSCs encapsulated in PEGDA hydrogel. Color images available online at www.liebertpub.com/tea

0.0005 mM (Fig. 2b). Conversely, ALP activity of hMSCs in the gel with peptide concentrations >0.0005 mM was significantly higher than the control that had no peptide (Fig. 2b). ALP activity after 14 days of incubation for the encapsulated hMSCs increased by 1.7- and 2.2-folds as the peptide concentration in the gel increased from 0.0005 to 0.005 mM, respectively. The rate of increase in ALP activity for the encapsulated hMSCs with above 0.0005 mM peptide concentration decreased with increasing peptide concentration, compared with concentrations in the 0.0005–0.005 mM range. A 1000-fold increase in peptide concentration from 0.005 to 5 mM increased ALP activity of the encapsulated hMSCs only by 1.4-fold at day 14 (Fig. 2b). ALP activity of the encapsulated hMSCs in the gel with 0.005 mM BMP-2 peptide was 2.4-fold higher than the control without peptide (Fig. 2b) after 14 days while that with 0.0004 mM BMP-2 protein (same weight concentration as peptide, 10 μg/mL) was 7.2-fold higher. The effect of peptide concentration on the extent of mineralization of encapsulated hMSCs (Fig. 2c), as measured by calcium content, was consistent with ALP activity. Calcium content of the encapsulated hMSCs at day 21 did not change significantly as the peptide concentration in the gel increased from 0 to 0.00025 and 0.0005 mM (Fig. 2c). The calcium content of hMSCs in the gel increased from 245 ± 50 to 340 ± 40 and 420 ± 50 mg/mg DNA as the peptide concentration increased by 5- and 10-fold, respectively, from 0.0005 to 0.0025 and 0.005 mM. Then, the calcium content of hMSCs increased at a slower rate from 420 ± 50 to 700 ± 100 mg/mg DNA with 500-fold increase in peptide concentration from 0.005 to 2.5 mM. Further increase in peptide concentration from 2.5 to 5 mM did not significantly change calcium content. The ALP and RunX-2 mRNA expression as a function of peptide concentration in Figure 2d and e, respectively, was consistent with ALP activities and calcium contents (Fig. 2b, c). Notably, the osteoinductive potential of BMP-2 peptide was significantly less than that of BMP-2 protein as the calcium content and ALP mRNA expression of hMSCs cultured with 10 μg BMP-2 protein/mL (0.0004 mM) were 4- and 12-fold higher than those cultured with the same 10 μg BMP-2 peptide/mL (0.005 mM), respectively. Further, RunX-2 expression of hMSCs cultured with BMP-2 protein (0.0004 mM, pink bar in Fig. 2e) and those cultured with BMP-2 peptide at the two highest concentrations (2.5 and 5 mM, light green and light blue) peaked on day 7 while those cultured with 0.005–0.5 mM peptide peaked on day 14. To summarize, the osteoinductive potential of BMP-2 peptide was significantly less than that of the protein and even 12,000-fold higher peptide molar concentrations could not achieve the osteoinductive potential of BMP-2 protein. Further, concentrations of 0.00025 and 0.0005 mM represented the low end of the BMP-2 peptide dose–response curve in osteogenic differentiation of hMSCs whereas concentration of 0.005 mM represented a level of stimulation approaching a plateau.

The results in Figure 2 prompted us to investigate stability of the peptide in aqueous solution. The hydrophobicity index for each amino acid, from N-terminus (left side) to C-terminus (right side) of the BMP-2 peptide, based on the difference in free energy of the aqueous and condensed phases[50] is shown in Figure 3a. The positive and negative

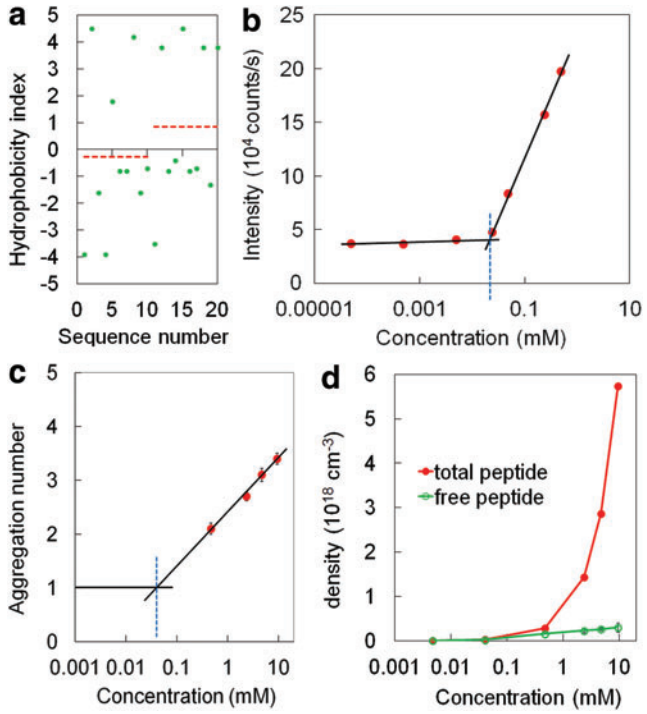

FIG. 3. **(a)** Hydrophobicity index for each amino acid from N-terminus (*left side*) to C-terminus (*right side*) of the BMP-2 peptide. **(b)** Intensity of scattered light as a function of peptide concentration in aqueous solution. **(c)** Simulated aggregation number of the BMP-2 peptide (number of peptides per aggregate) as a function of the peptide concentration in aqueous solution. **(d)** Density of the free BMP-2 peptide and total peptide density as a function of peptide concentration in aqueous solution. Color images available online at www.liebertpub.com/tea

indices indicate hydrophobic and hydrophilic residues, respectively. The distribution of hydrophobicity was not uniform along the peptide chain as the average hydrophobicity indices on N- (left) and C-terminus (right) sides of the peptide were −0.28 and 0.84, respectively (see the dash lines in Fig. 3a). Overall, the peptide was hydrophobic with an average hydrophobicity index of 0.28. The overall hydrophobicity suggested that the peptides formed aggregates in aqueous solution to reduce the overall free energy. Indeed, molecular dynamic simulations in Figure 3c show that the aggregation number (number of peptides per aggregate) increased with concentration of the peptide in aqueous solution. By extrapolating to aggregation number of one in Figure 3c, the CMC of 0.040 mM was obtained for the peptide. Similar to surfactants, the peptide is soluble in aqueous solution below CMC but it forms aggregates in equilibrium with the free peptide in solution above CMC with the propensity for aggregation increasing with peptide concentration.[51] CMC of the peptide was measured by DLS from the intersection of the two lines fitted to the scattered light intensity at high and low concentrations, as shown in Figure 3b. The intensity of scattered light did not change significantly at low concentrations in the absence of aggregation but it increased exponentially above CMC with aggregation. The experimentally measured CMC was 0.019 mM that was lower than the predicted value of 0.04 mM from simulations (Fig. 3c). The predicted higher CMC was most likely due to the error in extrapolating the aggregation number from higher concentrations to the aggregation of unity at CMC. However, the experimental and simulated CMCs were within the range of 0.005–0.05 mM, which was observed in the cell studies (Fig. 2). A lower rate of increase in ALP activity and calcium content for the encapsulated hMSCs with peptide concentration in the 0.005–0.05 mM range compared with the 0.0005–0.005 mM range can be attributed to the initiation of peptide aggregation (Fig. 2b, c). The predicted total and free peptide densities as a function of peptide concentration in solution are compared in Figure 3d. According to simulation results, the fraction of free peptide above CMC concentration decreased sharply from 0.54 to 0.16, 0.09, and 0.06 as the peptide concentration was increased from 0.5 to 2.5, 5, and 10 mM, respectively. However, the decrease in the free peptide fraction was offset by an increase in peptide number density. Therefore, the density of free peptide in solution increased by 1.9-folds from 0.16×10^{18} to 0.3×10^{18}/cm^3 while the total peptide density increased by 20-folds from 0.28×10^{18} to 5.73×10^{18}/cm^3 (Fig. 3d). The effect of peptide concentration, added to the gel and culture medium, on ALP activity (day 14) and calcium content (day 21) of hMSCs encapsulated in 15% PEGDA gel is shown in Figure 2b and c, respectively. Note that concentration scale in the figures is logarithmic. As the total peptide concentration was increased by 10-folds from 0.5 to 5 mM in a range well above CMC, ALP activity and calcium content increased by 1.1- and 1.2-folds, respectively, while the free peptide concentration increased by 1.6-fold from 0.26 to 0.42 mM (Supplementary Fig. S1; Supplementary Data are available online at www.liebertpub.com/tea). Therefore, the data suggest a better correlation between osteogenic activity and the free peptide concentration. Further, the significantly lower osteogenic activity of the peptide compared with BMP-2 protein, even at 12,000-fold higher concentration, was partially (see other effects due to peptide interaction with the cell membrane) attributed to aggregation in aqueous solution.

The effect of peptide hydrophobicity and its conjugation to the PEGDA network on DNA content, ALP activity, and calcium content of the encapsulated hMSCs is shown in Figure 4a–c, respectively. Groups included gels incubated in BM, OM without DEX, OM with peptide conjugated to the gel (cP), OM with peptide dissolved in the gel (P), and OM with peptide/lactide-capped PEG macromer with 0 (cPL0), 2 (cPL2), 4 (cPL4), and 6 (cPL6) lactides conjugated to the gel. DNA content of the encapsulated hMSCs cultured in BM increased with incubation time while those incubated in OM decreased, with or without peptide (Fig. 4a). The increase in DNA content in BM indicated that hMSCs were able to grow in the encapsulating PEGDA matrix but DNA content decreased with incubation time as the encapsulated cells underwent differentiation in OM consistent with previous reports.[52,53] Addition of BMP-2 peptide, peptide hydrophobicity, or peptide conjugation to the PEGDA matrix did not have a significant effect on cell number with incubation time.

ALP activity of the encapsulated hMSCs cultured in BM did not change with incubation time while those cultured in OM, with or without peptide, peaked on day 14. The

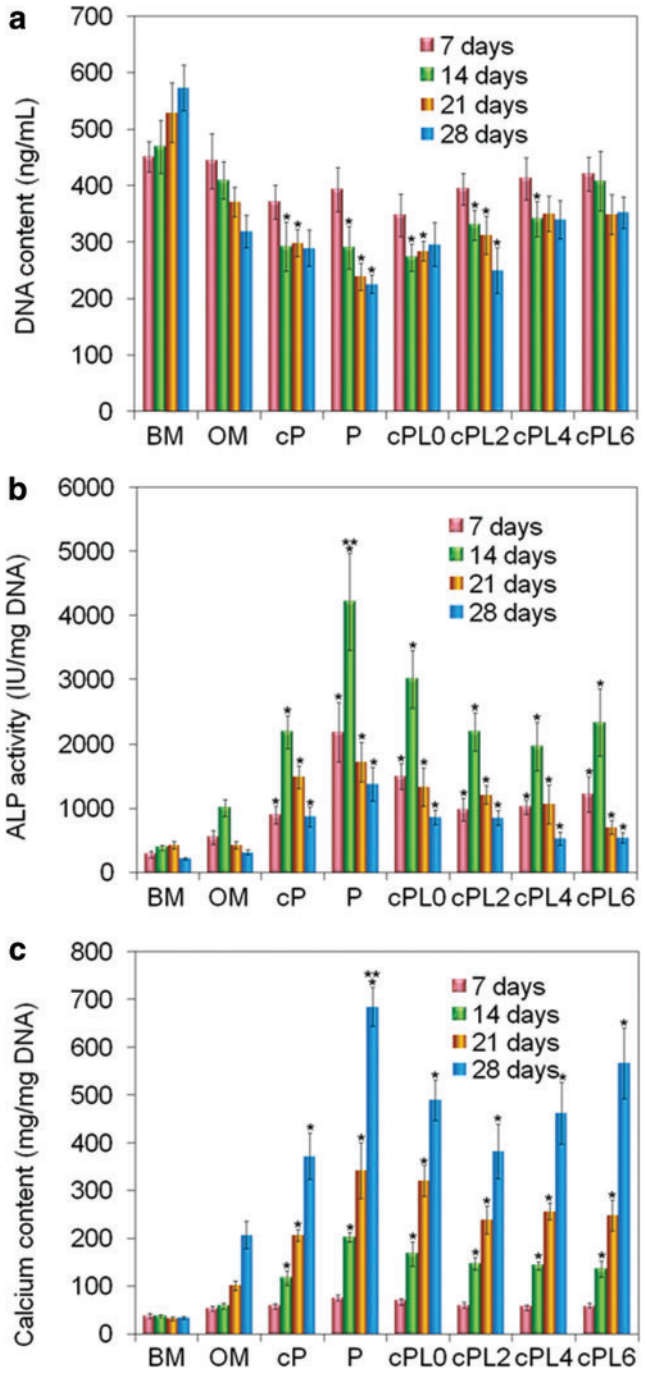

FIG. 4. DNA content **(a)**, ALP activity **(b)**, and calcium content **(c)** of hMSCs encapsulated in PEGDA hydrogel and incubated in basal medium (BM, control group), OM without DEX (control group), OM with the BMP-2 peptide covalently attached to the hydrogel network (cP), OM with the BMP-2 peptide dissolved in the hydrogel (P), OM with the peptide/lactide-capped PEG conjugate with 0 (cPL0), 2 (cPL2), 4 (cPL4), and 6 (cPL6) lactide units, attached to the hydrogel network. *One star* indicates a statistically significant difference ($p<0.05$) between the test and OM groups at each time point. *Two stars* indicate a statistically significant difference between the test and all other groups at each time point. Error bars correspond to means ± 1 standard deviation (SD) for $n=3$. Color images available online at www.liebertpub.com/tea

addition of BMP-2 peptide to the culture medium significantly increased the peak ALP activity on day 14, as shown by one star in Figure 4b. Further, the group with BMP-2 peptide dissolved in the medium (P) had significantly higher ALP activity on day 14 compared with those groups in which the peptide was conjugated to the PEGDA gel (cP, cPL0, cPL2, cPL4, and cPL6), as shown by two stars in Figure 4b. This is consistent with the fact that BMP-2 protein is associated with the soluble, not the insoluble, fraction of the bone matrix.[54] Further, ALP activity for cPL0 group (peptide-PEG conjugate attached to the gel) was 3000 ± 450 IU/mg DNA, which was higher than that for cP group (peptide attached to the gel) with 2200 ± 260 IU/mg DNA. Notably, ALP activity of the encapsulated hMSCs decreased when the PEG chain conjugated to the peptide was capped with a hydrophobic lactide segment (cPL2, cPL4, and CPL6 groups). However, the lactide segment length did not significantly change the peak ALP activity of the encapsulated hMSCs.

The extent of mineralization of hMSCs, as measured by calcium content, did not change with incubation time in BM but it increased in all OM groups (with or without peptide), as shown in Figure 4c. The addition of BMP-2 peptide to the gel (P group, Fig. 4c) significantly increased calcium content compared to that without peptide (OM medium, Fig. 4c). Consistent with ALP results, calcium content of the encapsulated hMSCs with dissolved peptide (P group) was 680 ± 40 mg/mg DNA, which was significantly higher than that conjugated to the gel (cP group, 370 ± 50 mg/mg DNA), as shown by two stars in Figure 4c. Extension of the peptide with a PEG chain increased calcium content of the encapsulated hMSCs from 370 ± 50 to 500 ± 40 mg/mg DNA at day 28. However, extension of the peptide with a lactide-capped PEG chain (lactide segment length of two, cPL2) significantly reduced calcium content at day 28 compared with PEG-extended peptide. The length of the lactide segment in lactide-capped PEG-conjugated peptide did not affect calcium content of the encapsulated hMSCs.

We hypothesized that the lower osteoinductive potential of the peptide groups conjugated to PEG or lactide-capped PEG was due to increased aggregation. The images in Figure 5 show the simulated equilibrium structure of BMP-2 peptide or peptide/lactide-capped PEG conjugates in aqueous solution (15 wt%). The blue and brown beads are for acrylate and lactide units, respectively, and EO beads are not shown for clarity. Figure 5a–g corresponds to acrylate-terminated (blue beads) PEG, lactide-capped PEG (two lactides, L2), PL0, PL2, PL4, and PL6, respectively. The acrylate-terminated PEG chains without lactide were uniformly distributed in the simulated aqueous solution, as shown by the acrylate beads in Figure 5a. PEG chains capped with lactide and terminated with an acrylate group formed micellar structures 1–3 nm in size as shown in Figure 5b,[22,25] with lactide and EO beads forming the core and corona of the micelles, respectively. The acrylate-terminated peptide without (Fig. 5c) or with conjugation to PEG (Fig. 5d) formed irregularly shaped aggregates (Fig. 5c, d) due to its amphiphilic nature. In the peptide case, hydrophobic side chains of the amino acids formed the core of the aggregates while EO beads covered surface of the aggregates with hydrophilic amino acids (polar and charged) positioned at the core-corona interface (Fig. 5d). The size of the aggregates increased when the peptide-PEG macromer was capped with

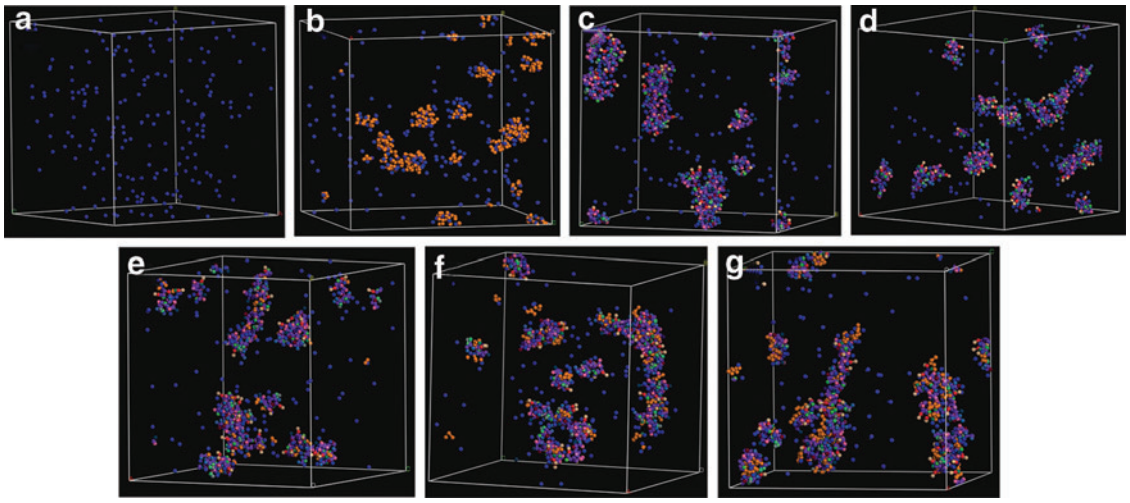

FIG. 5. Evolution of the BMP-2 peptide aggregates in PEGDA hydrogel (15 wt%) without the peptide or lactide-capped PEG macromer **(a,** control**)**, with lactide-capped PEG macromer **(b,** control, L0 group**)**, the peptide **(c,** P group**)**, the peptide-PEG conjugate **(d,** PL0 group**)**, the peptide/lactide-capped PEG conjugate with 2 **(e,** PL2 group**)**, 4 **(f,** PL4 group**)**, and 6 **(g,** PL6 group**)** lactides. The *blue* and *brown beads* correspond to acrylate and lactide beads, respectively. Ethylene oxide and water beads are not shown for clarity. Color images available online at www.liebertpub.com/tea

2, 4, and 6 lactide units as shown in Figure 5e–g, respectively, and the number density of the aggregates decreased with increasing lactide segment length. The cross-sections of one of the aggregates in the simulations of Figure 5 are shown in Figure 6 with green beads representing EO units. The cross-sections in Figure 6 show that the aggregates in aqueous solution are covered with EO units of PEG to reduce the interfacial free energy between the aqueous phase and hydrophobic structures, thus stabilizing the aggregates. Notably, thickness of the EO layer increased with aggregate size.

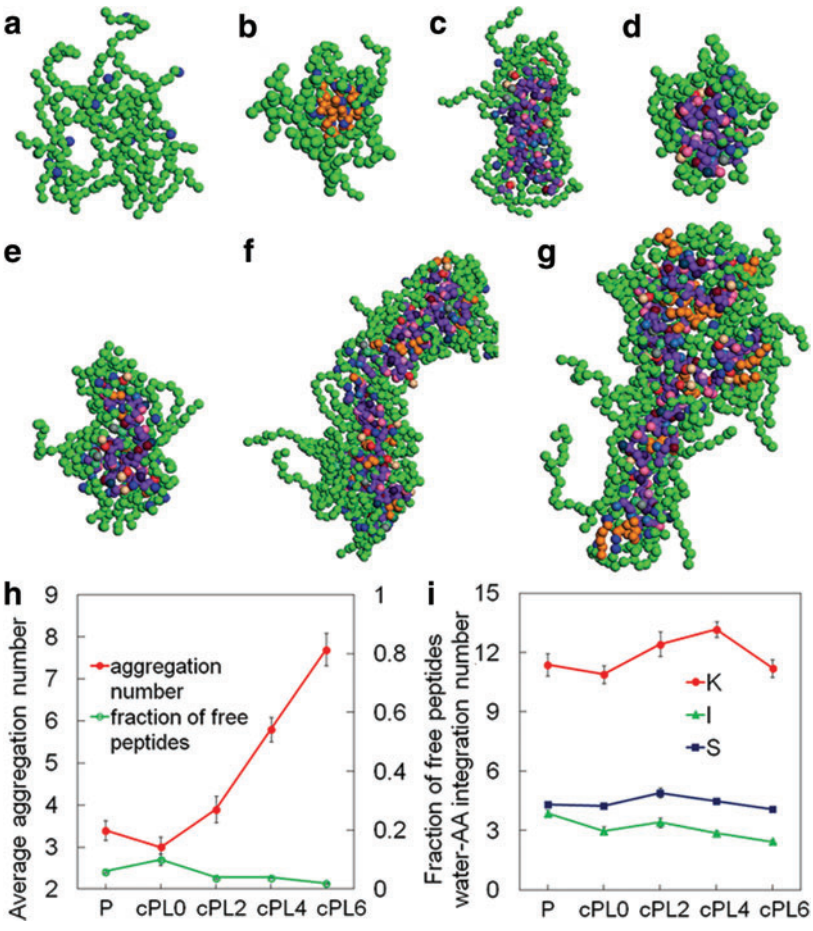

FIG. 6. Cross-section of one of the BMP-2 peptide aggregates in Figure 5 with *green beads* representing ethylene oxide units. Images **(a–g)** correspond to aggregates without the peptide or lactide-capped PEG macromer **(a)**, with lactide-capped PEG macromer **(b)**, the peptide **(c)**, peptide-PEG conjugate **(d)**, peptide/lactide-capped PEG conjugate with 2 **(e)**, 4 **(f)**, and 6 **(g)** lactides. Water beads are not shown for clarity. **(h)** Simulated average aggregation number and the fraction of free peptide **(h)** and the water-amino acid integration number for lysine (charged), serine (uncharged but polar), and isoleucine (nonpolar) **(i)** for the peptide only (P), the peptide-PEG conjugate attached to the hydrogel network (cPL0), the peptide/lactide-capped PEG conjugate attached to the gel network with 2 (cPL2), 4 (cPL4), and 6 (cPL6) lactide units. Error bars correspond to means ± SD for five simulation runs. Color images available online at www.liebertpub.com/tea

The average aggregation number (n_{agg}) and fraction of the free peptide (P) and peptide conjugated to lactide-capped PEG (cPL0, cPL2, cPL4, and cPL6) are shown in Figure 6h. Due to PEG hydrophilicity, n_{agg} decreased from 3.4 to 3.0 and aggregate distribution narrowed with conjugation of the peptide to PEG (cP). The n_{agg} increased from 3 to 3.9, 5.8, and 7.7 as the PEG macromer in peptide-PEG conjugate was capped with 2 (cPL2), 4 (cPL4), and 6 (cPL6) lactides, respectively. The n_{agg} increased from 3.4 to 4.3, 6.6, and 11.1 when the peptide was directly conjugated to lactide without PEG with segment length of 2, 4, and 6, respectively. On the other hand, the fraction of free peptide in solution increased from 0.06 to 0.1 with conjugation of the peptide to PEG (cP). Further, the fraction of free peptide decreased from 0.1 to 0.04, 0.03, and 0.02 for cPL2, cPL4, and cPL6, respectively.

To quantify the proximity of different beads, the average number of *b* beads in a sphere of radius *R* around bead *a* or the running integration number of beads *b* around bead *a*, IN_{ab} (*R*), was calculated by[22,25]

$$IN_{ab}(R) = 4\pi\rho_{b0}\int_0^R g_{ab}(r)r^2dr \qquad (6)$$

where ρ_{b0} is the overall number density of *b* beads and g_{ab} (*r*) is the radial distribution function of bead *b* around bead *a*, located at the origin. The integration numbers between water and amino acids lysine (K), serine (S), and isoleucine (I) representing charged, polar, and hydrophobic amino acids, respectively, are shown in Figure 6i. Isoleucine with lowest $IN_{AA\text{-}w}$ (green curve in Fig. 6i) was confined to the center of the aggregates while lysine with highest $IN_{AA\text{-}w}$ was situated on the aggregate surface in proximity to the PEG layer (Figs. 6b–g). The simulation results in Figure 6 indicated that, due to peptide aggregation, the encapsulated hMSCs may interact with the PEG layer on the surface of peptide-PEG aggregates or amino acids different from the BMP-2 peptide sequence, leading to a lower osteoinductive potential of the lactide-capped PEG-conjugated peptide.

The effect of peptide aggregation on interaction with the cell membrane was simulated by molecular dynamics and the results are shown in Figure 7. When a single peptide (not an aggregate) or a single peptide-PEG conjugate was in contact with the cell membrane, the distance between the center of masses of the peptide and cell membrane did not change significantly. However, when an aggregate of the BMP-2 peptides (P, upper left and right images) or an aggregate of the peptide-PEG conjugates (PL0, lower left and right images) was in contact with the cell membrane, higher energetic interaction, penetration of the peptide, and pore formation in the membrane were observed. However, conjugation of the peptide to PEG (PL0) reduced the attractive interaction between the conjugate and the cell membrane and the extent of pore formation. Notably, covalent attachment of the peptide-PEG conjugate to the hydrogel network eliminated pore formation in the cell membrane.

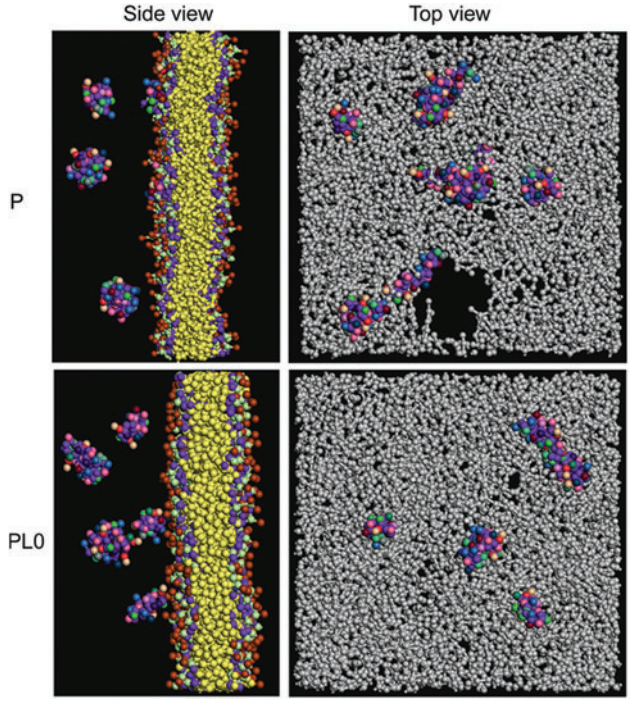

FIG. 7. Effect of an aggregate of the BMP-2 peptide (*top images*) and an aggregate of the peptide-PEG conjugate (*bottom images*) on energetic interaction, penetration of the peptide, and pore formation in the cell membrane. The water beads are not shown for clarity. The images on the *left* and *right* show the *side* and *top* views of the membrane, respectively. In the *top* view, all membrane beads are shown in *gray* for clarity. Color images available online at www.liebertpub.com/tea

Discussion

Aside from cost efficiency, osteogenic peptides are less likely to lose their activity by denaturation than their corresponding protein. Therefore, a wider range of methods can be used for incorporation of osteogenic peptides in engineered scaffolds. Li *et al.* measured osteoinductivity of the BMP-2 peptide loaded in nano-hydroxy apatite/collagen/poly(L-lactic acid) scaffolds by implantation in a rat calvarial defect.[55] They reported that 3 mg of the BMP-2 peptide loaded in the scaffold had osteoinductive potential similar to 1 μg of BMP-2 protein, indicating that 3000-fold higher BMP-2 peptide concentrations were required to achieve the same activity as the protein. Our results demonstrate that although the addition of the BMP-2 peptide significantly increased osteoinductive potential, the level of activity was much less than that of BMP-2 protein even at 12,000-fold higher molar concentrations (1000-fold higher mass concentrations). Further, the expression of RunX-2, a marker for the onset of osteogenic differentiation, was delayed with the BMP-2 peptide compared with BMP-2 protein (Fig. 2e). One factor that can lower osteoinductive potential of the peptide is aggregation in aqueous solution. On the other hand, the peptide is derived from BMP-2 protein based on its ability to differentiate MSCs to osteogenic lineage without consideration for its stability in aqueous solution. Hydrophobicity index analysis of each amino acid indicated that the peptide is amphiphilic with an overall positive index of hydrophobicity. Therefore, the peptide tends to form aggregates above its CMC in aqueous solution to reduce the interfacial free energy. The BMP-2 peptide concentration range of 0.00025–0.005 mM was

below the peptide's CMC concentration of 0.019 mM (or 0.040 mM based on the simulation results). Therefore, based on the experimental and simulated values for CMC, the peptides in cell encapsulation experiments with 0.00025–0.005 mM concentrations were most likely not aggregated. Above CMC concentration, the fraction of free peptide decreased with increasing peptide concentration but the free peptide density in the hydrogel slightly increased, which could explain the slight increase in osteoinductive potential with increasing peptide concentration in Figure 2. Therefore, the experimental and computational results indicate that osteoinductive potential of the BMP-2 peptide is related to the density of free or nonaggregated peptide in aqueous solution, not the overall concentration. Further, simulation results show that the amino acids in the peptide aggregates facing the aqueous phase may be different from those of the free peptide (Fig. 6i), which may lead to nonspecific interaction of the aggregates with cell surface receptors. In addition, simulation results in Figure 7 show that the peptide aggregates (P) had a higher energy of interaction with the cell membrane than the free peptide, leading to undesired pore formation on the membrane and reduced peptide activity. When the peptide was conjugated to PEG (PL0), the peptide aggregates were shielded from the cell membrane by surface-bound PEG chains, which slightly increased peptide activity. This is consistent with previous results that palmitoylation of proapoptotic peptides can affect micelle stability and cell uptake.[56]

The results show that there was higher osteogenic differentiation of encapsulated hMSCs when the BMP-2 peptide was dissolved in the hydrogel matrix as compared with the peptide that was conjugated (Fig. 4), which was similar to the previously reported lower activity of BMP-2 protein attached to immobilized heparin.[57] Conjugation of the peptide to the hydrophilic PEGDA matrix decreased the degree of freedom of the peptide beads, which decreased aggregation and increased the free peptide density. Further, capping the PEG chain with hydrophobic lactide units increased aggregation number of the conjugated peptide, which was attributed to a decrease in CMC. The free energy of micelle formation is related to CMC by[51,58]

$$\Delta G^0_{mic} = RT \ln (CMC) \tag{7}$$

where R and T are the gas constant and absolute temperature, respectively, and ΔG^0_{mic} is the difference in free energy of the peptide between the dissolved and aggregated states. CMC and ΔG^0_{mic} increased with conjugation of the peptide to hydrophilic PEG, leading to an increase in free peptide concentration and higher osteoinductive potential of the PEG-conjugated peptide (cPL0) compared with cP. However, the addition of hydrophobic lactide units to the PEG-peptide conjugate offsets the positive effect of PEG conjugation to the peptide, leading to an insignificant change in osteoinductive potential of cPL2, cPL4, and cPL6 groups compared with cPL0.

Conclusions

In this work, the effect of concentration and hydrophobicity of the BMP-2 peptide, from residues 73–92 of the knuckle epitope of BMP-2 protein, on differentiation of hMSCs encapsulated in PEGDA hydrogel was investigated experimentally and by molecular dynamic simulation. The encapsulated cells were cultured in OM without DEX supplemented with the BMP-2 peptide. The index of hydrophobicity of the peptide was varied by conjugation to a lactide-capped PEG chain with 0–6 lactide units. The BMP-2 peptide dissolved in the hydrogel had significantly higher osteoinductive potential than the attached peptide consistent with the fact that BMP-2 protein is associated with the soluble, not the insoluble, fraction of the bone matrix. The dose-osteogenic response curve of the BMP-2 peptide was in the 0.0005–0.005 mM range, and osteoinductive potential of the BMP-2 peptide was significantly less than the protein even at 12,000-fold higher molar concentrations, which was explained by peptide aggregation in aqueous solution. Based on simulation results, the fraction of free peptide in solution decreased while the concentration of free peptide increased slightly with 1000-fold increase in peptide concentration in aqueous solution, which reduced osteoinductive potential of the peptide. A decrease in the index of hydrophobicity of the peptide by conjugation to PEG increased CMC, which increased osteoinductive potential of the peptide. Conversely, an increase in the index of hydrophobicity of the peptide by conjugation to lactide-capped PEG reduced CMC, which reduced the peptide osteoinductive potential. Experimental and simulation results indicated that osteoinductive potential of the BMP-2 peptide should be correlated with its hydrophobicity index, CMC concentration in aqueous medium, and the concentration of free peptide in solution, not the total peptide concentration.

Acknowledgments

This work was supported by research grants to J.E. from the National Science Foundation under grant Nos. CBET0756394, CBET0931998, DMR1049381, and IIP-1357109; the National Institutes of Health under grant Nos. DE19180 and AR063745; the Arbeitsgemeinschaft Fur Osteosynthesefragen (AO) Foundation under grant No. C10-44J; and University of South Carolina Office of VP for Research under grant No. 15510-E414. The authors thank Mr. Joshua D. Walters and Mr. John W. Sieracke for assistance with peptide and hydrogel synthesis.

Disclosure Statement

No competing financial interests exist.

References

1. Mckay, W.F., Peckham, S.M., and Badura, J.M. A comprehensive clinical review of recombinant human bone morphogenetic protein-2 (INFUSE Bone Graft). Int Orthop **31,** 729, 2007.
2. McKay, B., and Sandhu, H.S. Use of recombinant human bone morphogenetic protein-2 in spinal fusion applications. Spine (Phila Pa 1976) **27,** S66, 2002.
3. Carragee, E.J., Hurwitz, E.L., and Weiner, B.K. A critical review of recombinant human bone morphogenetic protein-2 trials in spinal surgery: emerging safety concerns and lessons learned. Spine J **11,** 471, 2011.
4. Yang, H.S., La, W.G., Bhang, S.H., Jeon, J.Y., Lee, J.H., and Kim, B.S. Heparin-conjugated fibrin as an injectable system for sustained delivery of bone morphogenetic protein-2. Tissue Eng Part A **16,** 1225, 2010.

5. Mercado, A.E., and Jabbari, E. Effect of encapsulation or grafting on release kinetics of recombinant human bone morphogenetic protein-2 from self-assembled poly(lactide-co-glycolide ethylene oxide fumarate) nanoparticles. Micros Res Tech **73,** 824, 2010.
6. Mercado, A.E., Ma, J., He, X., and Jabbari, E. Release characteristics and osteogenic activity of recombinant human bone morphogenetic protein-2 grafted to novel self-assembled poly(lactide-co-glycolide fumarate) nanoparticles. J Control Rel **140,** 148, 2009.
7. Shields, L.B.E., Raque, G.H., Glassman, S.D., Campbell, M., Vitaz, T., Harpring, J., and Shields, C.B. Adverse effects associated with high-dose recombinant human bone morphogenetic protein-2 use in anterior cervical spine fusion. Spine (Phila Pa 1976) **31,** 542, 2006.
8. Raida, M., Clement, J.H., Leek, R.D., Ameri, K., Bicknell, R., Niederwieser, D., and Harris, A.L. Bone morphogenetic protein 2 (BMP-2) and induction of tumor angiogenesis. J Cancer Res Clin **131,** 741, 2005.
9. Jabbari, E. Osteogenic peptides in bone regeneration. Curr Pharm Design **19,** 3391, 2013.
10. Kirsch, T., Sebald, W., and Dreyer, M.K. Crystal structure of the BMP-2-BRIA ectodomain complex. Nat Struct Biol **7,** 492, 2000.
11. Liu, F., Ventura, F., Doody, J., and Massague, J. Human type-II receptor for bone morphogenic proteins (BMPs)—extension of the 2-kinase receptor model to the BMPs. Mol Cell Biol **15,** 3479, 1995.
12. Saito, A., Suzuki, Y., Ogata, S., Ohtsuki, C., and Tanihara, M. Activation of osteo-progenitor cells by a novel synthetic peptide derived from the bone morphogenetic protein-2 knuckle epitope. Biochim Biophys Acta **1651,** 60, 2003.
13. Saito, A., Suzuki, Y., Ogata, S., Ohtsuki, C., and Tanihara, M. Accelerated bone repair with the use of a synthetic BMP-2-derived peptide and bone-marrow stromal cells. J Biomed Mater Res A **72A,** 77, 2005.
14. Zhang, S.M., Greenfield, M.A., Mata, A., Palmer, L.C., Bitton, R., Mantei, J.R., Aparicio, C., de la Cruz, M.O., and Stupp, S.I. A self-assembly pathway to aligned monodomain gels. Nat Mater **9,** 594, 2010.
15. Anderson, J.M., Andukuri, A., Lim, D.J., and Jun, H.W. Modulating the gelation properties of self-assembling peptide amphiphiles. ACS Nano **3,** 3447, 2009.
16. Luo, J.N., and Tong, Y.W. Self-assembly of collagen-mimetic peptide amphiphiles into biofunctional nanofiber. ACS Nano **5,** 7739, 2011.
17. Ellis-Behnke, R.G., Liang, Y.X., You, S.W., Tay, D.K.C., Zhang, S.G., So, K.F., and Schneider, G.E. Nano neuro knitting: peptide nanofiber scaffold for brain repair and axon regeneration with functional return of vision. Proc Natl Acad Sci U S A **103,** 7530, 2006.
18. Santoso, S., Hwang, W., Hartman, H., and Zhang, S.G. Self-assembly of surfactant-like peptides with variable glycine tails to form nanotubes and nanovesicles. Nano Lett **2,** 687, 2002.
19. Moeinzadeh, S., and Jabbari, E. Mesoscale simulation of the effect of a lactide segment on the nanostructure of star poly(ethylene glycol-co-lactide)-acrylate macromonomers in aqueous solution. J Phys Chem B **116,** 1536, 2012.
20. Marrink, S.J., de Vries, A.H., and Mark, A.E. Coarse grained model for semiquantitative lipid simulations. J Phys Chem B **108,** 750, 2004.
21. Monticelli, L., Kandasamy, S.K., Periole, X., Larson, R.G., Tieleman, D.P., and Marrink, S.J. The MARTINI coarse-grained force field: extension to proteins. J Chem Theory Comput **4,** 819, 2008.
22. Moeinzadeh, S., Barati, D., Sarvestani, S.K., Karaman, O., and Jabbari, E. Nanostructure formation and transition from surface to bulk degradation in polyethylene glycol gels chain-extended with short hydroxy acid segments. Biomacromolecules **14,** 2917, 2013.
23. Moeinzadeh, S., Khorasani, S.N., Ma, J., He, X., and Jabbari, E. Synthesis and gelation characteristics of photo-crosslinkable star Poly (ethylene oxide-co-lactide-glycolide acrylate) macromonomers. Polymer (Guildf) **52,** 3887, 2011.
24. He, X., Ma, J., and Jabbari, E. Effect of grafting RGD and BMP-2 protein-derived peptides to a hydrogel substrate on osteogenic differentiation of marrow stromal cells. Langmuir **24,** 12508, 2008.
25. Moeinzadeh, S., Barati, D., He, X., and Jabbari, E. Gelation characteristics and osteogenic differentiation of stromal cells in inert hydrolytically degradable micellar polyethylene glycol hydrogels. Biomacromolecules **13,** 2073, 2012.
26. White, P., Keyte, J.W., Bailey, K., and Bloomberg, G. Expediting the Fmoc solid phase synthesis of long peptides through the application of dimethyloxazolidine dipeptides. J Pept Sci **10,** 18, 2004.
27. Kaiser, E., Colescott, R.L., Bossinger, C.D., and Cook, P.I. Color test for detection of free terminal amino groups in the solid-phase synthesis of peptides. Anal Biochem **34,** 595, 1970.
28. Jabbari, E., Yang, X., Moeinzadeh, S., and He, X. Drug release kinetics, cell uptake, and tumor toxicity of hybrid VVVVVVKK peptide-assembled polylactide nanoparticles. Eur J Pharm Biopharm **84,** 49, 2013.
29. Yang, S.J., and Zhang, S.G. Self-assembling behavior of designer lipid-like peptides. Supramol Chem **18,** 389, 2006.
30. Khoe, U., Yang, Y.L., and Zhang, S.G. Self-assembly of nanodonut structure from a cone-shaped designer lipid-like peptide surfactant. Langmuir **25,** 4111, 2009.
31. Sarvestani, A.S., Xu, W., He, X., and Jabbari, E. Gelation and degradation characteristics of *in situ* photo-crosslinked poly (l-lactide-co-ethylene oxide-co-fumarate) hydrogels. Polymer (Guildf) **48,** 7113, 2007.
32. Meinel, A.J., Kubow, K.E., Klotzsch, E., Garcia-Fuentes, M., Smith, M.L., Vogel, V., Merkle, H.P., and Meinel, L. Optimization strategies for electrospun silk fibroin tissue engineering scaffolds. Biomaterials **30,** 3058, 2009.
33. Chung, E.J., Chien, K.B., Aguado, B.A., and Shah, R.N. Osteogenic potential of BMP-2-releasing self-assembled membranes. Tissue Eng Part A **19,** 2664, 2013.
34. Henderson, J.A., He, X., and Jabbari, E. Concurrent differentiation of marrow stromal cells to osteogenic and vasculogenic lineages. Macromol Biosci **8,** 499, 2008.
35. Livak, K.J., and Schmittgen, T.D. Analysis of relative gene expression data using real-time quantitative PCR and the 2(T)(-Delta Delta C) method. Methods **25,** 402, 2001.
36. Pfaffl, M.W. A new mathematical model for relative quantification in real-time RT-PCR. Nucleic Acids Res **29,** e45, 2001.
37. Brocos, P., Mendoza-Espinosa, P., Castillo, R., Mas-Oliva, J., and Pineiro, A. Multiscale molecular dynamics simulations of micelles: coarse-grain for self-assembly and atomic resolution for finer details. Soft Matter **8,** 9005, 2012.
38. Gkeka, P., and Sarkisov, L. Interactions of phospholipid bilayers with several classes of amphiphilic alpha-helical peptides: insights from coarse-grained molecular dynamics simulations. J Phys Chem B **114,** 826, 2010.

39. Zhang, H., Wang, H., Xu, G.Y., and Yuan, S.L. A molecular dynamics simulation of N-(fluorenyl-9-methoxycarbonyl)-dipeptides supramolecular hydrogel. Colloids Surf A Physicochem Eng Asp **417,** 217, 2013.
40. Santo, K.P., and Berkowitz, M.L. Difference between magainin-2 and melittin assemblies in phosphatidylcholine bilayers: results from coarse-grained simulations. J Phys Chem B **116,** 3021, 2012.
41. Yang, S.C., and Faller, R. Pressure and surface tension control self-assembled structures in mixtures of pegylated and non-pegylated lipids. Langmuir **28,** 2275, 2012.
42. Lee, H., and Pastor, R.W. Coarse-grained model for pegylated lipids: effect of pegylation on the size and shape of self-assembled structures. J Phys Chem B **115,** 7830, 2011.
43. Martyna, G.J., Klein, M.L., and Tuckerman, M. Nose-Hoover chains: the Canonical ensemble via continuous dynamics. J Chem Phys **97,** 2635, 1992.
44. Materials Studio V 5.5. San Diego, CA: Accelrys, 2011.
45. Marrink, S.J., Risselada, H.J., Yefimov, S., Tieleman, D.P., and de Vries, A.H. The MARTINI force field: coarse grained model for biomolecular simulations. J Phys Chem B **111,** 7812, 2007.
46. Gobin, A.S., and West, J.L. Effects of epidermal growth factor on fibroblast migration through biomimetic hydrogels. Biotechnol Prog **19,** 1781, 2003.
47. DeLong, S.A., Moon, J.J., and West, J.L. Covalently immobilized gradients of bFGF on hydrogel scaffolds for directed cell migration. Biomaterials **26,** 3227, 2005.
48. Swiontkowski, M.F., Aro, H.T., Donell, S., Esterhai, J.L., Goulet, J., Jones, A., Kregor, P.J., Nordsletten, L., Paiement, G., and Patel, A. Recombinant human bone morphogenetic protein-2 in open tibial fractures—a subgroup analysis of data combined from two prospective randomized studies. J Bone Joint Surg Am **88A,** 1258, 2006.
49. Mygind, T., Stiehler, M., Baatrup, A., Li, H., Zoua, X., Flyvbjerg, A., Kassem, M., and Bunger, C. Mesenchymal stem cell ingrowth and differentiation on coralline hydroxyapatite scaffolds. Biomaterials **28,** 1036, 2007.
50. Kyte, J., and Doolittle, R.F. A simple method for displaying the hydropathic character of a protein. J Mol Biol **157,** 105, 1982.
51. Owen, S.C., Chan, D.P.Y., and Shoichet, M.S. Polymeric micelle stability. Nano Today **7,** 53, 2012.
52. Oliveira, J.M., Sousa, R.A., Kotobuki, N., Tadokoro, M., Hirose, M., Mano, J.F., Reis, R.L., and Ohgushi, H. The osteogenic differentiation of rat bone marrow stromal cells cultured with dexamethasone-loaded carboxymethylchitosan/poly(amidoamine) dendrimer nanoparticles. Biomaterials **30,** 804, 2009.
53. Wang, L.M., Dormer, N.H., Bonewald, L.F., and Detamore, M.S. Osteogenic differentiation of human umbilical cord mesenchymal stromal cells in polyglycolic acid scaffolds. Tissue Eng Part A **16,** 1937, 2010.
54. Scheufler, C., Sebald, W., and Hülsmeyer, M. Crystal structure of human bone morphogenetic protein-2 at 2.7 Å resolution. J Mol Biol **287,** 103, 1999.
55. Li, J.F., Hong, J.J., Zheng, Q.X., Guo, X.D., Lan, S.H., Cui, F.Z., Pan, H.T., Zou, Z.W., and Chen, C. Repair of rat cranial bone defects with nHAC/PLLA and BMP-2-related peptide or rhBMP-2. J Orthop Res **29,** 1745, 2011.
56. Missirlis, D., Khant, H., and Tirrell, M. Mechanisms of peptide amphiphile internalization by SJSA-1 cells *in vitro*. Biochemistry **48,** 3304, 2009.
57. Ruppert, R., Hoffmann, E., and Sebald, W. Human bone morphogenetic protein 2 contains a heparin-binding site which modifies its biological activity. Eur J Biochem **237,** 295, 1996.
58. Zana, R. Critical micellization concentration of surfactants in aqueous solution and free energy of micellization. Langmuir **12,** 1208, 1996.

Address correspondence to:
Esmaiel Jabbari, PhD
Biomimetic Materials and Tissue Engineering Laboratory
Department of Chemical Engineering
University of South Carolina
Swearingen Engineering Center
Rm 2C11
Columbia, SC 29208

E-mail: jabbari@mailbox.sc.edu

Received: December 23, 2013
Accepted: June 25, 2014
Online Publication Date: September 30, 2014